Circumvention of Fluorophore Photobleaching in Fluorescence Fluctuation Experiments: a Beam Scanning Approach

Dmitri Satsoura,[b] Brian Leber,[b] David W. Andrews,[b] and Cécile Fradin*[a, b]

Photobleaching is a fluorophore-damaging process that commonly afflicts single-molecule fluorescence studies. It becomes an especially severe problem in fluorescence fluctuation experiments when studying slowly diffusing particles. One way to circumvent this problem is to use beam scanning to decrease the residence time of the fluorophores in the excitation volume. We report a systematic study of the effects of circular beam scanning on the photobleaching of fluorescent particles as observed in single-photon excitation fluorescence fluctuation experiments. We start by deriving a simple expression relating the average detected fluorescence to the photobleaching cross section of the fluoro-phores. We then perform numerical calculations of the spatial distribution of fluorescent particles in order to understand under which conditions beam scanning can prevent the formation of a photobleaching hole. To support these predictions, we show experimental results obtained for large unilamellar vesicles containing a small amount of the fluorescent lipophilic tracer DiD. We establish the required scanning radius and frequency range in order to obtain sufficient reduction of the photobleaching effect for that system. From the detected increase in fluorescence upon increase in scanning speed, we estimate the photobleaching cross section of DiD.

Introduction

Biophysical methods for single-molecule analysis have recently attracted a growing interest among biochemists and biologists.[1] Because of their relative ease of application for the study of biological molecules in solution and in the cellular environment, fluorescence-based methods are now widely used in the life sciences, leading to unprecedented results at the molecular level.[2] Fluorescence fluctuation methods, which rely on the statistical analysis of the spatial or temporal fluctuations of the fluorescence signal, stand out among several single-molecule analysis methods. These fluorescence-based methods provide the means to follow the dynamics of a multitude of biologically relevant processes, such as diffusion,[3,4] velocity,[5] rotation,[6] conformational changes,[7] and protein–protein interactions.[8] The analysis of the fluorescence fluctuations is usually done in one of two ways. The first is to consider the autocorrelation function (ACF) of the fluorescence signal, as done, for example, in fluorescence correlation spectroscopy[3,9] (FCS) and image correlation spectroscopy.[10] The second is to consider the photon-counting histogram[11,12] (PCH), as done, for example, in fluorescence intensity distribution analysis (FIDA).[13]

A crucial requirement for fluorescence-based methods is the availability of an adequate fluorophore to label the biological molecule of interest. In general, such a fluorophore should not perturb the biological function of the molecule, its specific brightness should be as high as possible, and it should be photostable. In particular, it should be resistant to photobleaching, a process defined as the irreversible light-induced destruction of the fluorophore. Photobleaching is often due to reaction of the excited-state fluorophore with another mole-

cule. Thus, this common drawback is intimately related to the very process that makes fluorescent molecules useful. Although progress is constantly being made towards improving the photostability of available organic fluorophores and fluorescent proteins, they are all still subject to photobleaching. At the moment, quantum dots are the only fluorescent probes that are truly resistant to photobleaching, yet their blinking, toxicity and bulky size makes them less than ideal probes for some applications.

In fluorescence fluctuation measurements, fluorophores are observed while they diffuse through the tight focus of a laser beam where the photon flux is very high. Quickly diffusing fluorescent particles such as dyes are unlikely to photobleach during the short time they usually spend in the laser focus. The situation, however, is different for particles that diffuse slowly. As the use of fluorescence fluctuation techniques extends to slower particles, for example large molecular complexes, vesicles, or membrane proteins, and to different environments, for example viscous media such as polymer gels, concentrated solutions, or cells, the probability for fluoro-

[a] Dr. C. Fradin
Department of Physics and Astronomy
McMaster University
1280 Main Street West, Hamilton, ON, L8S4M1 (Canada)
Fax: (+1) 905-546-1252
E-mail: fradin@physics.mcmaster.ca

[b] D. Satsoura, Dr. B. Leber, Dr. D. W. Andrews, Dr. C. Fradin
Department of Biochemistry and Biomedical Sciences
McMaster University
1200 Main Street West, Hamilton, ON, L8N3Z5 (Canada)

phores to photobleach while under observation increases. This is an important issue, because the interpretation of fluorescence fluctuation measurements is model-dependent, and photobleaching effects are not always easy to recognize and correct for. Fluorescence fluctuation measurements are affected by photobleaching in two ways: 1) Photobleaching of fluorophores while they reside in the detection volume immediately results in a reduced average number of detected fluorescent particles and in a reduced apparent residence time in the detection volume. We refer to this effect as short-term photobleaching. 2) Over the course of a measurement, photobleaching throughout the light cone (single-photon excitation) or at the laser focus (multi-photon excitation) results in a progressive decrease of the total number of fluorescent particles present in the sample and in a nonuniform concentration of fluorophores. We refer to this effect as long-term photobleaching. The influence of short-term photobleaching on the ACF has been approximated successfully as a steady-state process.[14, 15] On the other hand, no detailed description of the influence of photobleaching on the PCH is available, although computer simulations suggest that it might be important.[16] Long-term photobleaching results in non-steady state effects, with the result that the forms of both the ACF and PCH depend on the duration of the measurement. For measurements performed in closed compartments, such as cells that contain only a limited pool of fluorophores, the decrease in the total number of fluorescent particles, reflected in a decrease in the fluorescence count rate, becomes especially noticeable.[17–19] Methods have been proposed to correct for this effect when calculating the ACF[20] or the PCH.[21]

Herein, we explore the potential of beam scanning as a way to reduce the effects of photobleaching in fluorescence fluctuation experiments. We focus our efforts on circular beam scanning, which has the advantage of being easily implemented and of not resulting in significant modifications of the ACF and PCH. Linear and circular beam scanning have been used in conjunction with FCS or PCH methods to improve the signal-to-noise ratio,[22] to study the oligomerization of slowly diffusing particles,[23] to increase the visibility of rare particles,[24–27] and to study membrane dynamics.[28] In several cases, beam (or sample) scanning was also presented as a way to reduce photobleaching.[22, 27, 29, 30] It was noted that scanning could increase both the measured concentration and molecular brightness of the detected fluorophore,[26, 27] and this approach was found to be especially useful in the case of slowly diffusing particles.[22, 26, 29] However, these effects have not yet been studied in detail. We start by briefly summarizing the different theoretical approaches that have been used to describe the effect of photobleaching on fluorescence fluctuation measurements. We then develop a simple theoretical framework to understand how circular beam scanning will modify the output of these measurements. The first part of this framework deals with short-term photobleaching effects, and we derive a simplified expression for the average detected fluorescence as a function of the beam scanning speed and of the concentration, diffusion coefficient, and photobleaching cross section of the fluorophores. We then turn our attention to long-term

photobleaching effects. Assuming that the laser focus is acting as a sink for fluorescent particles, we numerically calculate the sample's particle distribution, obtained as a result of linear and circular beam scanning. We also discuss which range of scanning parameters can be used to avoid the formation of a photobleaching hole. We subsequently use large unilamellar lipid vesicles (LUVs), made fluorescent by the introduction of a small fraction of the lipophilic tracer DiD to the membrane, as a model experimental system for testing the reduction of photobleaching in the presence of beam scanning as observed in FCS and FIDA experiments. We show that photobleaching can be eliminated by scanning the beam at a sufficient speed and by making appropriate choices for the scanning radius and frequency. Finally, we estimate the photobleaching cross section of the DiD fluorophore from analysis of the average fluorescence signal recorded as a function of scanning speed.

Experimental Section

Materials: Lipids were purchased from Avanti Polar Lipids (Alabaster, AL, USA). Phosphatidylcholine (PC) and phosphatidylethanolamine (PE) were purified from egg. Phosphatidylinositol (PI) was from bovine liver. Phosphatidylserine (PS) and cardiolipin (CL) were purchased as synthetic lipids in the dioleoyl (DO) or tetraoleoyl (TO) forms, respectively. HEPES [4-(2-hydroxyethyl)-1-piperazineethanesulfonic acid] was obtained from BioShop Canada Inc. (Burlington, Ontario, Canada). The fluorescent carbocyanine dye 1,1′-dioctadecyl-3,3,3′,3′-tetramethylindodicarbocyanine, 4-chlorobenzenesulfonate salt (DiD) and the fluorescent dye Alexa Fluor 633 C_5-maleimide (Alexa 633) were purchased from Molecular Probes (Eugene, OR, USA). Other chemicals were purchased from Sigma–Aldrich (Oakville, Ontario, Canada).

LUV Preparation: Large unilamellar vesicles (LUVs) were prepared from PC, PE, PI, DOPS and TOCL, with a mass ratio of 48:28:10:10:4. A small fraction (0.002%) of the lipophilic dye DiD was added as a tracer. Lipids and lipophilic tracers were mixed in the appropriate ratios from stock solutions dissolved in chloroform and methanol, respectively. The organic solvents were removed by evaporation under a stream of nitrogen gas, followed by incubation (2 h) under vacuum to remove traces of solvent. Dry lipid films were then resuspended in liposome buffer (10 mM HEPES at pH 7.4, 200 mM KCl, 5 mM $MgCl_2$, 0.2 mM EDTA), subjected to 10 freeze–thaw cycles, and extruded through a 100 nm Nucleopore polycarbonate membrane (Nucleopore, San Diego, CA, USA).

Fluorescence Fluctuation Instrument: Fluorescence fluctuation measurements were carried out using an Insight Research Spectrometer (Evotec Technologies, Hamburg, Germany). The configuration of the instrument allows recording autocorrelation functions and photon counting histograms in parallel and permits beam scanning. For fluorescence excitation, we used a 637 nm continuous-wave laser diode (Radius 635-25, Coherent, Santa Clara, CA, USA). The laser beam is attenuated by neutral density filters, passes a beam expander, and is directed into the microscope objective (40×, 1.15 N.A. Olympus U-APO, water immersion objective) via a dichroic mirror and a scanning mirror. Fluorescence collected by the same objective is focused onto a confocal pinhole (70 μm) to eliminate out-of-focus fluorescence. Afterwards, the light is passed through a spectral band-pass filter before reaching the photon-counting detector (SPCM-CD3017, Perkin–Elmer Optoelectronics, Wellesley, MA, USA). The inclination of the scanning mirror

placed just before the objective is controlled by a set of two piezo-electric actuators (S-334, Physik Instrumente, Karlsruhe, Germany), providing the instrument with beam-scanning capacity. The piezo-electric actuators allow for a maximum ± 25 mrad tilt of the mirror with µrad resolution (corresponding to a ± 50 mrad tilt of the laser beam and to a ± 170 µm lateral displacement of the laser focus away from the optical axis) in either the x or the y direction. The high resonant frequency of the mirror–piezoelectric actuators system (≈ 1 kHz) allows for periodic scanning of the laser focus at a frequency up to 100 Hz. The actuators are interfaced to a PC via a piezo control system (E-501, Physik Instrumente). Setting the frequency and amplitude of the two actuators to the same value results in circular scanning.

Fluorescence Fluctuation Measurements: The Alexa 633 dye or fluorescently labeled LUVs were diluted in liposome buffer at nanomolar (Alexa) or subnanomolar (LUVs) concentration, and samples (200 µL) were applied to a 96-well microplate with coverslip bottom (Whatman Inc., Brentford, UK) placed on the fluorescence fluctuation instrument. The laser beam was focused 150 µm above the surface of the coverslip. All measurements were performed at room temperature. Unless otherwise stated, measurements were recorded for a period of 10 s, and each measurement was repeated 10 times, thus error bars correspond to the standard deviation of 10 measurements. Data analysis for the ACFs was carried out with the software KaleidaGraph (Synergy Software, Reading, PA, USA). Data analysis for the PCHs was carried out with the software Acapella (Evotec Technologies, Hamburg, Germany), which uses the FIDA method.

Numerical Calculations: Numerical calculations were performed using the software Maple (Maplesoft, Waterloo, Ontario, Canada).

Theory

Fluorescence Fluctuation Spectroscopy in the Absence of Photobleaching

In standard fluorescence fluctuation spectroscopy experiments, the fluorescence signal $F(t)$ coming from a small immobile detection volume is collected and its temporal fluctuations are analyzed by analysis of the autocorrelation function (for FCS) or photon-counting histogram (for FIDA). The average fluorescence, or count rate, $<F(t)>$, measured in these experiments is related to the average number of fluorophores present in the detection volume, N, and to their specific brightness, B, defined as the average number of photons detected per fluorophore and per second. In the case of a single fluorescent species:

$$\langle F(t) \rangle = NB. \tag{1}$$

The autocorrelation function, $G(\tau)$, is defined by [Eq. (2)]:[31]

$$G(\tau) = \frac{\langle F(t)F(t+\tau) \rangle}{\langle F(t) \rangle^2} - 1, \tag{2}$$

and the photon-counting histogram, $\Pi(k,\delta)$, refers to the probability of detecting exactly k photons during a time interval δ.[11,12] These two functions extract different information from the signal. The ACF is sensitive to the dynamics and concentration of the fluorescent particles, while the PCH is sensitive to their specific brightness and their concentration, but not their dynamics.

In the case of a single fluorescent species with diffusion coefficient D, and assuming a 3D Gaussian detection volume with $1/e^2$ radius w_0 and $1/e^2$ height z_0, the ACF takes the analytical form given in Equation (3):[3]

$$G_D(\tau) = \frac{1/N}{\left(1 + \tau/\tau_D\right)\sqrt{1 + \tau/S^2\tau_D}} \left[1 + \frac{T}{1-T}\exp\left(-\frac{\tau}{\tau_T}\right)\right], \tag{3}$$

where $\tau_D = w_0^2/4D$ is the characteristic diffusion time, $S = z_0/w_0$ is the detection volume aspect ratio, and τ_T and T are the relaxation time associated with triplet state and the average fraction of fluorophores found in that state, respectively. In the limit of large aspect ratios ($S \gg 1$), τ_D corresponds to the average time necessary for a particle to escape the detection volume when starting from a random location in that volume.

The shape of the PCH is governed by super-Poissonian statistics; two types of phenomena cause variations in the number of photons detected during consecutive time intervals: 1) fluctuation of the number of molecules in the detection volume and 2) fluctuation of the number of fluorescence photons detected from each of these molecules.[12] In the case of one-photon excitation, the detection volume is not perfectly approximated by a Gaussian profile. Thus, no simple analytical form adequately describes the PCH. Instead, a very large number of convolutions must be performed to retrieve the exact photon distribution $\Pi(k,\delta)$. To efficiently handle the convolution operations, FIDA, which is a numerical method that relies on the use of generating functions, was introduced.[13] To further facilitate the rapid evaluation of $\Pi(k,\delta)$, the spatial profile of the detection volume is taken into account through two effective parameters, A_0 and A_1. These parameters are determined experimentally by fitting the PCH for a solution containing a single well-characterized fluorescent dye. They play much the same role as the effective aspect ratio S, which is generally obtained by fitting the ACF obtained for a fluorescent dye with Equation (3).

Modification of the ACF and PCH in the Presence of Circular Beam Scanning

If the laser beam used for fluorophore excitation scans across the sample, the ACF given above [Eq. (3)] is no longer valid. For circular beam scanning, a modified expression for the ACF has been calculated for two-photon excitation[25] and can be adapted to one-photon excitation by replacing w_0 in the original expression with $\sqrt{2}w_0$ to account for the altered definition of w_0 in the case of two-photon excitation. For a beam scanned along a circular trajectory of radius R at a frequency f, this leads to Equation (4):

$$G(\tau) = G_D(\tau) \exp\left\{ -\frac{2R^2[1 - \cos(2\pi f\tau)]}{w_0^2\left(1 + \tau/\tau_D\right)} \right\}. \tag{4}$$

At low scanning frequencies ($2\pi f \ll 1/\tau_D$), Equation (4) simplifies to Equation (5):

$$G(\tau) = G_D(\tau) \exp\left[-\frac{\left(\tau/\tau_s\right)^2}{\left(1 + \tau/\tau_D\right)} \right], \tag{5}$$

where the characteristic scanning time $\tau_s = w_0/(2\pi fR)$ has been introduced. This expression is similar to that obtained for particles subjected to a flow,[32] except that the quantity $v = 2\pi fR = w_0/\tau_s$ represents the speed of the laser focus and not the flow velocity.

In contrast to the ACF, the PCH should not be affected by beam scanning in the absence of photobleaching as long as the sampling time δ used to construct the PCH remains much shorter than the particle residence time, $\delta \ll \tau_s$.

Modification of the ACF and PCH because of Short-Term Photobleaching

For a given set of conditions, photobleaching can be characterized by the rate at which fluorophores are destroyed. Because photobleaching usually occurs from fluorophore excited states, the photobleaching rate strongly depends on the light flux and is consequently not uniform across the detection volume. For the purpose of discussing the effects of short-term photobleaching, however, it is useful to define an effective average photobleaching rate for the detection volume, k_P. When $1/k_P < \tau_D$, the fluorescent particles will, on average, be detected for a duration $\tau_P = 1/k_P$, after which they photobleach and become nonfluorescent. The apparent residence time of the particles in the detection volume, which determines the characteristic decay time of the ACF, then approaches τ_P instead of τ_D. At the same time, the apparent average number of particles detected in the detection volume decreases. A modified expression for the ACF taking into account this short-term photobleaching process (and based on the approximation of a uniform photobleaching rate across the detection volume), Equation (6), has been used by several groups:[15,16,33]

$$G(\tau) = G_D\left\{ 1 + A\left[\exp\left(-\tau/\tau_P\right) - 1\right] \right\}. \tag{6}$$

Due to the simplifying assumption of a uniform k_P, the ACF behaves as if only a fraction A of the particles is affected by photobleaching. While one study provides a theoretical justification for $A \approx 0.8$ in agreement with measurements,[15] the exact value of this parameter will depend somewhat on experimental conditions, for example on the exact form of the excitation profile.

Short-term photobleaching also affects the PCH, because it decreases the total number of fluorescence photons. Numerical simulations have shown that the analysis of PCHs obtained

for particles subjected to photobleaching should return values for the fluorophore concentration and specific brightness which are smaller than the actual values.[16] These simulations also showed that even in the case of severe photobleaching, the PCH for a single fluorophore species still obeys super-Poissonian statistics, at least in appearance.[16]

## Effect of Short-Term Photobleaching on Average Count Rate

To assess the effect of short-term photobleaching on the average count rate, we make the approximation that the detection volume is uniformly illuminated. This allows the use of the same effective photobleaching rate k_P that was introduced in the previous section. At least at low excitation power, I, this rate should be proportional to the light energy flux, $\Phi = I/\pi w_0^2$. More specifically:[15]

$$k_P = \frac{\sigma_P \lambda}{hc} \Phi \tag{7}$$

where σ_P is the effective photobleaching cross-section, λ is the excitation wavelength, h is Planck's constant and c is the speed of light. For a fluorophore entering a uniformly illuminated area at time $t = 0$, the probability of still being fluorescent at time t depends on the lifetime associated with the photobleaching process, $\tau_P = 1/k_P$, and is given by $\exp(-t/\tau_P)$. Therefore, the average fluorescence intensity F collected from N fluorophores with specific brightness B spending a time τ_R in the detection volume is [Eq. (8)]:

$$F = \frac{NB}{\tau_R} \int_{t=0}^{t=\tau_R} \exp\left(-t/\tau_P\right) dt = \frac{NB\tau_P}{\tau_R}\left[1 - \exp\left(-\tau_R/\tau_P\right)\right] \tag{8}$$

The variation of F with τ_P is shown in Figure 1. If the characteristic time associated with photobleaching, τ_P, is much larger
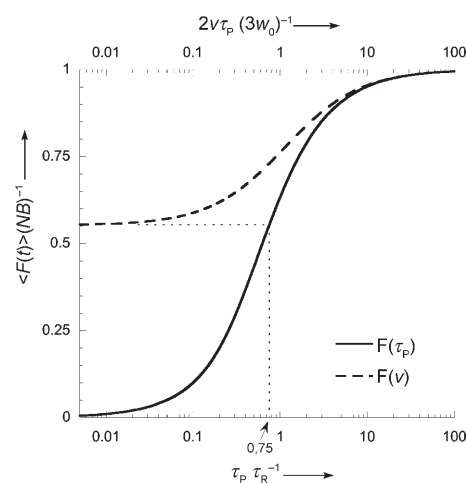
Figure 1. Expected average normalized fluorescence, $<F(t)> (NB)^{-1}$, as a function of normalized photobleaching characteristic time, $\tau_P\tau_R^{-1}$ [——, calculated according to Eq. (8)]. The same curve is also shown as a function of normalized scanning speed, $2v\tau_P/(3w_0)$, in order to demonstrate the range of intensities that can be observed experimentally in the case when $\tau_P = \tau_D$ [– – –, calculated according to Eq. (10)].

than the residence time of the particles in the detection volume, τ_R, short-term photobleaching effects are negligible, and we recover $F = NB$. On the other hand, if $\tau_P \approx \tau_R$, then a fraction of the N fluorophores in the detection volume is photobleached and $F < NB$; in particular, $F = NB/2$ for $\tau_P \approx \tau_R/1.594$. Finally, F goes to zero for $\tau_P \ll \tau_R$. Although we made simplifying assumptions about the light distribution in the detection volume, a comparison between Equation (8) and a more precise estimate of the same quantity obtained through numerical simulations[34] shows that the approximations made to obtain Equation (8) conserve the correct form for F while yielding a simple analytical function.

Dependence of the Average Count Rate on Scanning Speed

For beam scanning, the residence time of a diffusing particle in the detection volume can be approximated by:

$$\tau_R = 1 \left/ \left(\frac{1}{\tau'_D} + \frac{1}{\tau'_S} \right) \right. \tag{9}$$

where τ'_D is the average residence time in the detection volume of a diffusing particle in the absence of beam scanning, and τ'_S is the average residence time of an immobile particle in the presence of beam scanning. Note that τ'_D is not identical to the characteristic diffusion time $\tau_D = w_0^2/4D$. While τ'_D is, by definition, the average total residence time of the particles in the experimental detection volume (from the moment they enter to the moment they exit), τ_D corresponds to the average escape time from an hypothetical detection volume with infinite aspect ratio for particles starting from a random location in that volume. So these two quantities are slightly different, with τ_D being independent of S, while τ'_D weakly depends on S. In the case of a sphere ($S = 1$), $\tau'_D = 4\tau_D/3$, while for a cylinder $\tau'_D = \tau_D \times \ln(2S)$.[24] Similarly, τ'_S and τ_S are slightly different quantities. If the detection volume is a sphere, it is easy to show that $\tau'_S = 3\tau_S/2$. By inserting Equation (9) in Equation (8) and assuming the limit of detection volumes with small aspect ratio ($S \approx 1$), we obtain the average count rate expected as a function of scanning speed [Eq. (10)]:

$$F(v) = NB\tau_P \left(\frac{3}{4\tau_D} + \frac{2v}{3w_0} \right) \left\{ 1 - \exp\left[-\frac{1}{\tau_P \left(\frac{3}{4\tau_D} + \frac{2v}{3w_0} \right)} \right] \right\} \tag{10}$$

This expression is plotted in Figure 1 assuming that N does not depend on the scanning speed, that is, assuming that long-term photobleaching effects are negligible. This assumption, however, does not always hold true, as discussed below. When it does, and when $k_P/1.594 > 3/(4\tau_D)$, the count rate reaches half its maximum value at the scanning speed $v_P = (3w_0/2) \times (k_P/1.594 - 3/4\tau_D)$. Thus v_P represents a crossover value for the beam velocity: If $v \ll v_P$ short-term photobleaching effects are dominant, and if $v \gg v_P$ they are negligible.

Long-Term Photobleaching Effects: Linear Beam Scanning

We have so far neglected long-term photobleaching effects, taking into account neither the photobleaching occurring outside of the detection volume nor the modification of the concentration profile due to diffusion of photobleached molecules outside of the illuminated area. The fact that photobleaching in single-photon excitation occurs throughout the light cone, that is, also above and below the laser focus, means that the diffusion of photobleached molecules should be treated as a two-dimensional problem.[18,34] Therefore, we model the effect of photobleaching on the particle distribution in the focal plane, $C(x,y)$, by solving the two-dimensional diffusion equation in the presence of a continuous sink placed at the position of the laser focus. We first consider linear beam scanning and look for steady-state solutions to the diffusion equation for a sink with constant speed, v. In the referential linked to the sink, the time-independent diffusion equation is:

$$\frac{\partial^2 C}{\partial x^2} + \frac{\partial^2 C}{\partial y^2} = -\frac{v}{D} \frac{\partial C}{\partial x}. \tag{11}$$

If a sink destroying particles at an effective rate α is placed at the origin, Equation (11) is valid everywhere except at the origin. The presence of the sink is reflected in a boundary condition stating that the flux of particles around the origin must be $-\alpha$. Note that α represents a global destruction rate for the total volume of the sink. For example, for a uniform photobleaching process occurring at an effective rate k_P across an area V where the fluorophore concentration is C, we would have $\alpha = CVk_P$. Taking into account this boundary condition, the solution to Equation (11) is given in Equation (12):

$$C(x,y) = C_0 - \frac{\alpha}{2\pi D} K_0 \left(\frac{v\sqrt{x^2 + y^2}}{2D} \right) \exp(-vx/2D) \tag{12}$$

where K_0 is the modified Bessel function of the second kind and zeroth order, and C_0 is the particle concentration in the absence of the sink. The resulting 2D concentration is shown in Figure 2a, and the concentration profile along the x-axis is shown in Figure 2b. In front of the sink ($x > 0$), the particle concentration increases sharply over the characteristic length $2D/v$ because of the exponential factor in Equation (12). Behind the sink ($x < 0$), the concentration increases only slowly, a reflection of the fact that the sink is leaving a trail of photobleached particles behind it.

If the sink is turned on at time $t = 0$, the particle distribution at time t, before the steady state is reached, can be obtained by integrating the Green function for the diffusion equation over the trajectory of the sink. In the referential linked to the sink we obtain Equation (13):

$$C(x,y,t) = C_0 - \int_0^t \frac{\alpha}{4\pi Du} \exp\left[-\frac{(x + vu)^2 + y^2}{4Du} \right] du \tag{13}$$
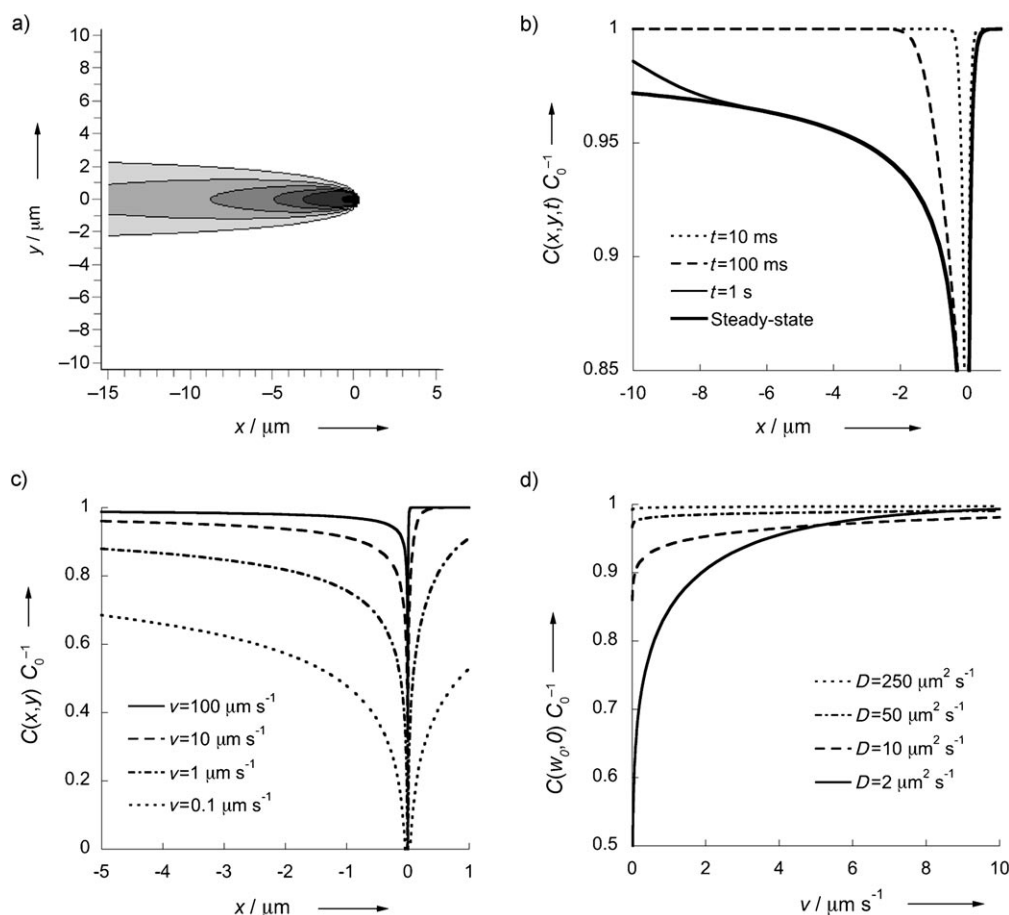
Figure 2. Linearly moving sink. a) Steady-state concentration profile $C(x,y)$ in the referential linked to the sink ($v = 10\ \mu m\,s^{-1}$, $D = 1\ \mu m^2 s^{-1}$, $\alpha/C_0 = 1\ \mu m^2 s^{-1}$). The contours represent reduction in concentration of 1%, 2%, 3%, 4%, 5% and 10% compared to the reference concentration C_0. b) Establishment of the photobleaching hole, as evidenced by the normalized particle distribution along the trajectory of the sink, shown for different times after the sink was turned on, and compared to the steady-state distribution ($v = 10\ \mu m\,s^{-1}$, $D = 1\ \mu m^2 s^{-1}$, $\alpha/C_0 = 1\ \mu m^2 s^{-1}$). c) Influence of scanning speed on the shape and depth of the photobleaching hole ($D = 1\ \mu m^2 s^{-1}$, $\alpha/C_0 = 1\ \mu m^2 s^{-1}$). d) Normalized apparent concentration, $C(w_0,0)/C_0$, shown as a function of beam velocity ($w_0 = 0.5\ \mu m$, $\alpha/C_0 = 1\ \mu m^2 s^{-1}$).

This integral does not have a simple analytical solution, except when t goes to infinity, in which case $C(x,y,t)$ becomes equal to the steady-state solution $C(x,y)$. Several transient particle distributions are shown in Figure 2b for comparison with the steady-state solution. It takes only a very short time, $\approx D/v^2$, for the sharp particle gradient present in front of the sink to be established (corresponding to the time necessary for the particles to diffuse over the distance $2D/v$). On the other hand, the tail is established only progressively, and its length, $\approx vt$, increases linearly with time.

The shape of the steady-state particle distribution depends only on the value of v/D, while the magnitude of the photobleaching "hole" caused by the sink depends separately on v, D, and, of course, α. When the velocity of the sink increases, the particle distribution becomes more and more asymmetric, while the overall amplitude of the photobleaching hole diminishes. Both effects act to reduce the influence of long-term photobleaching (Figure 2c). A large diffusion coefficient, while making the particle distribution more symmetric, also decreases the depth of the photobleaching hole. Thus, quickly diffus-

ing particles will have a lesser tendency to form a photobleaching hole than slowly diffusing particles.

In a beam-scanning experiment, we are interested in the concentration of fluorescent particles found immediately in front of the detection area, $C(w_0,0)$, because this concentration determines the incoming flux of fluorescent particles in the detection volume and consequently the value of the parameter N [Eq. (8)]. The parameter $C(w_0,0)$, called the apparent particle concentration, is plotted in Figure 2d as a function of beam velocity. It increases sharply above the critical velocity $v_c = 2D/w_0$ at which the particle distribution starts decaying over a distance shorter than w_0 in front of the sink. For $v < v_c$, the laser focus does not move forward as fast as the photobleached particles diffusing in front of it, so the detection volume remains in the photobleaching hole and the apparent particle concentration is lower than the real concentration. On the other hand, for $v > v_c$ the beam moves forward faster than already photobleached particles, and the apparent particle concentration is equal to the real particle concentration.

In conclusion, long-term photobleaching effects can be avoided by linearly scanning the beam or the sample at a velocity larger than the critical velocity $v_c = 2D/w_0$, which prevents the formation of a region with decreased fluorescent particle concentration around the detection volume (photobleaching hole).

Long-term Photobleaching Effects: Circular Beam Scanning

In contrast to a sink moving linearly, there is no steady-state solution in two dimensions for a sink moving in a circular fashion. We then need to consider transient solutions, which we obtain by integrating the Green function for the diffusion equation over the trajectory of the sink. For a sink rotating about the origin with radius R and frequency f, having started photobleaching particles at $t = 0$, and found in $(x,y) = (R,0)$ at t, the distribution of fluorescent particles is given by Equation (14):

$$C(x,y,t) = C_0 -$$
$$\int_0^t \frac{\alpha}{4\pi Du} \exp\left\{ -\frac{[x - R\cos(2\pi fu)]^2 + [y + R\sin(2\pi fu)]^2}{4Du} \right\} du$$

(14)

This particle distribution is shown in Figure 3. The circularly moving sink leaves a trail of nonfluorescent particles in its wake (Figure 3a), as in the case for a sink moving linearly. After one rotation period, the sink starts "biting its tail" and catching up with the nonfluorescent particles it created earlier (Figure 3b). After a very short transient during which the front is established (which, by analogy with the linear motion case, must happen for $t < D/v^2$), and after a longer transient during which the tail is established ($t < 1/f$), the particle concentration along the sink trajectory keeps decreasing regularly without changing its shape significantly, (Figure 3c). As a result, the particle concentration found immediately in front of the sink, $C(R,w_0)$, decreases slowly with time during a circular scanning experiment. In addition, a sudden drop in particle concentration is observed each time the beam completes a full circle (Figure 3c, inset). Once the critical velocity at which the front is established is reached ($v_c = 2D/w_0$, or $f_c = D/\pi Rw_0$), the primary effect of further increasing the frequency for a fixed scanning radius and scan duration is to slightly decrease the apparent particle concentration along the beam trajectory, since fluorophores have less and less time to diffuse away before the beam completes a full circle (Figure 3d). This effect becomes important for $f > f_t = 1/\tau_D$. Increasing the scanning radius for a fixed scanning frequency also affects the apparent number of particles. Again, the first effect should be the topping of the critical velocity ($v_c = 2D/w_0$, obtained for $R_c = D/\pi fw_0$). The second effect, equally striking, is escaping the photobleaching hole. For very small scanning radii, a symmetric photobleaching hole is established, as in the case of an immobile source, so that even above the critical velocity the apparent concentration can be significantly smaller than the real sample concentration (Figure 3e). To better illustrate that effect, Figure 3f shows the apparent particle concentration as a function of

scanning radius for a constant velocity, which gives an indication of the amplitude and range of the photobleaching hole. Both keep increasing with time, in particular the hole radius scales as $R_h = \sqrt{4Dt}$, and the apparent particle concentration will critically depend on whether R is smaller than R_h.

The main conclusion that can be drawn from these calculations in the case of circular scanning is that, as in the case of linear scanning, the principal requirement in order to avoid long-term photobleaching is the use of a scanning velocity larger than the critical velocity $v_c = 2D/w_0$. In addition, to ensure that the scanning conditions will prevent the beam from returning too quickly to regions where the fluorescent particle concentration has been depleted, the scanning frequency has to be lower than $f_t = 1/\tau_D$, and the scanning radius has to be larger than the photobleaching hole radius $R_h = \sqrt{4Dt}$.

We note that our modeling relies on two important simplifications. The first simplification is that we have assumed the global rate α at which particles are photobleached to be constant. Yet α depends on the concentration of particles in the detection volume ($\alpha = CVk_P$), which in the presence of beam scanning can be compared to the concentration particles found right in front of the beam, $C(w_0,0)$. In non-steady state situations where $C(w_0,0)$ is time-dependant, $\alpha \approx C(w_0,0)Vk_P$ is also time-dependent, and the shape of the solutions we have calculated is not exact. Since fluorescent particle concentration tends to decrease with time due to photobleaching, we expect the effective photobleaching rate α to decrease with time in these situations, in turn reducing the rate at which fluorophore concentration decreases. Thus by considering α to be constant, we overestimate the importance of non-steady state effects such as the slow concentration decrease illustrated in Figure 3c. All our conclusions, however, remain qualitatively correct. Indeed, non-steady state effects similar to the ones we predict here have been predicted for comparable systems (photobleaching in a biological membrane in the absence of beam scanning) using more sophisticated modeling.[19] The second simplification is that while we have considered a point source in our calculations, the photobleaching area is extended in a real experiment. This means that the solutions we obtain are different from the exact solution close to the sink. Considering the exact light distribution would eliminate the divergence at the sink observed in our calculations, but would not change the conclusions drawn from our simple model.

Results and Discussion

Characterization of Photobleaching from the Fluorescence Fluctuation Data

To illustrate the influence of photobleaching on the output of fluorescence fluctuation experiments, we carried out FCS and FIDA measurements for the small organic dye Alexa 633 both with and without circular beam scanning. We varied the light energy flux at the laser focus in the range 0–70 kW cm^{-2}. Representative ACFs and PCHs are shown in Figures 4a and b, and
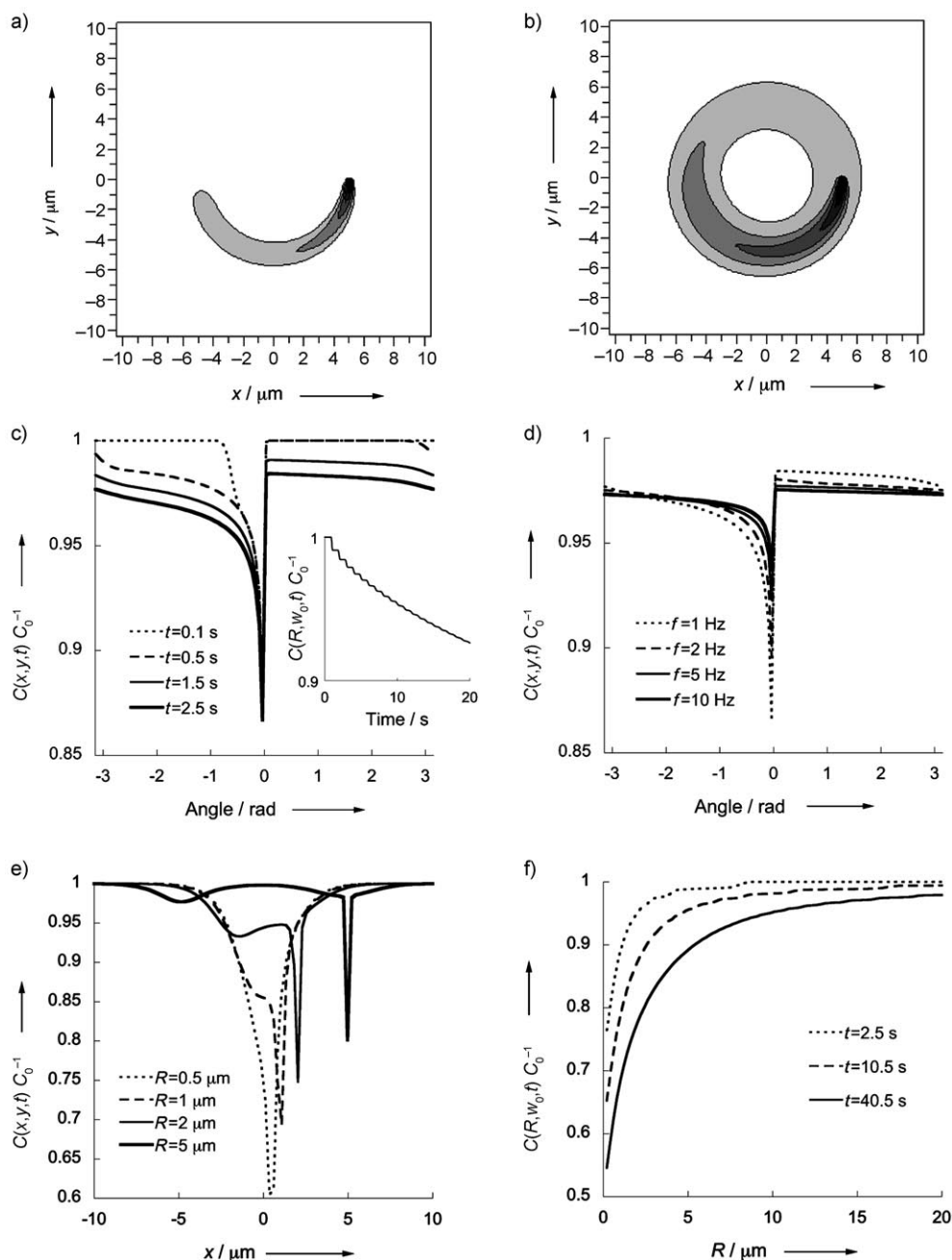
Figure 3. Circularly moving sink. a) Concentration profile $C(x,y,t)$ for a sink rotating around the origin after $t = 0.5$ s. b) Concentration profile $C(x,y,t)$ for a sink rotating around the origin after $t = 2.5$ s. For (a) and (b), $f = 1$ Hz, $R = 5$ μm, $D = 1$ μm²s⁻¹, $\alpha/C_0 = 1$ μm²s⁻¹; the contours represent reduction in concentration of 1 %, 2 %, 3 %, 4 %, 5 % and 10 % compared to the reference concentration C_0. c) Normalized concentration profile along the sink trajectory for different scan durations. Inset: change in the apparent particle concentration, $C(R,w_0)$, with time ($f = 1$ Hz, $R = 5$ μm, $D = 1$ μm²s⁻¹, $\alpha/C_0 = 1$ μm²s⁻¹). d) Influence of change in scanning frequency on the particle concentration ($R = 5$ μm, $D = 1$ μm²s⁻¹, $\alpha/C_0 = 1$ μm²s⁻¹), as shown by changes in the particle distribution along the sink trajectory (calculated for $t = 2.5$ s). e) Influence of the scanning radius on the particle concentration ($f = 1$ Hz, $D = 1$ μm²s⁻¹, $\alpha/C_0 = 1$ μm²s⁻¹, $t = 2.5$ s), as shown by changes in the particle distribution along the x-axis. f) Normalized apparent particle concentration as a function of scanning radius at constant velocity ($v = 20$ μm s⁻¹, $D = 1$ μm²s⁻¹, $\alpha/C_0 = 1$ μm²s⁻¹).

parameters obtained from the fit of the autocorrelation data are shown in Figures 4c and d.

Upon increasing the excitation power, the ACFs obtained without beam scanning (Figure 4a, black curves) are affected by two competing effects. For $\Phi \lesssim 20$ kW cm⁻², the characteristic decay time of the ACF progressively shifts towards longer lag times owing to optical saturation.[35] Further increasing the

excitation power results in a shift of the decay time towards shorter lag times, presumably due to photobleaching.[15] This effect is captured in the dependence of the apparent characteristic diffusion time τ_D obtained by fitting the ACFs with a simple diffusion model [Eq. (3)], and shown in Figure 4c. The characteristic decay time increases for Φ up to 20 kW cm⁻² and decreases afterwards. If photobleaching is taken into account
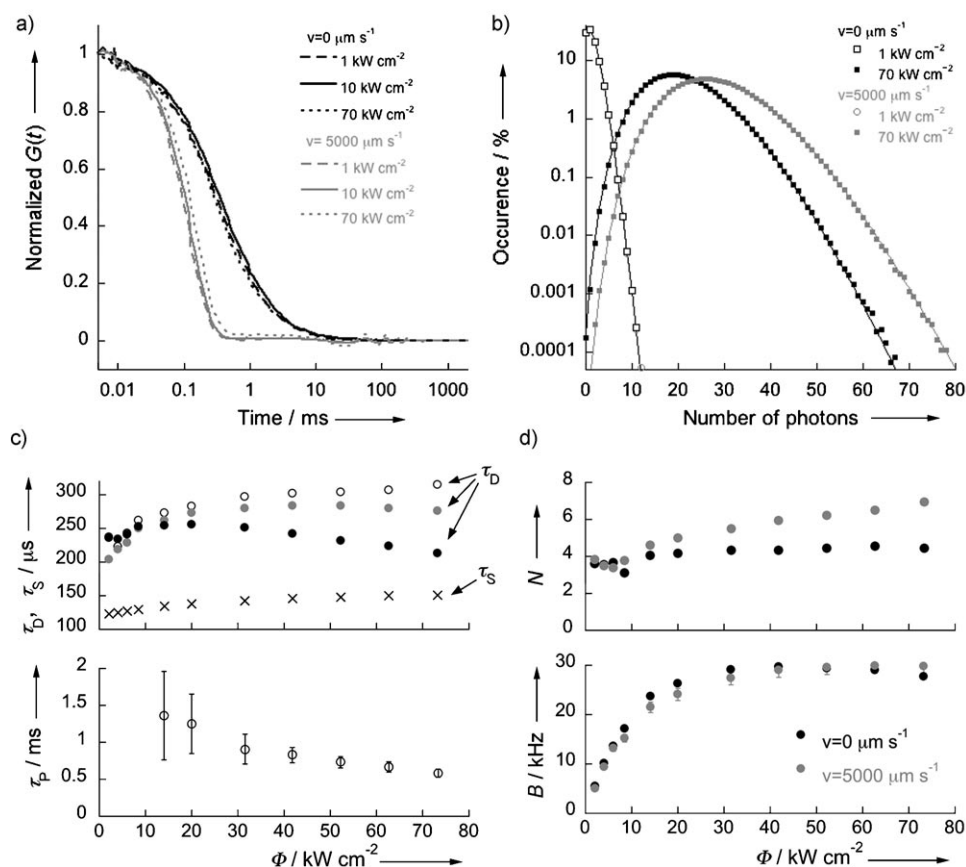
Figure 4. Correlation data obtained for the dye Alexa 633. a) Autocorrelation functions and b) photon counting histograms recorded without (black lines and symbols) and with (gray lines and symbols) beam scanning ($f = 15.9$ Hz, $R = 50$ μm). All curves are representative 5 min measurements. Thick lines and symbols correspond to experimental data. Thin lines correspond to fit as explained in the text. c) Characteristic times obtained from the fit of the ACFs. Upper panel: characteristic diffusion times τ_D obtained from fitting the ACFs in the absence of beam scanning using either Equation (3) (●) or Equation (6) (○) compared to the characteristic diffusion time τ_D and characteristic scanning time τ_S obtained by fitting the ACFs in the presence of beam scanning using Equation (5) (● and ×, respectively). Lower panel: characteristic photobleaching time obtained from fitting the ACFs in the absence of beam scanning using Equation (6). d) Parameters obtained from the fit of the PCHs. Upper panel: average number of fluorescent particles in the detection volume. Lower panel: specific brightness of the fluorescent particles.

model [Eq. (5)]. The radius of the detection volume, w_0, can be calculated from τ_S since $w_0 = v\tau_S$. w_0 is found to increase steadily from 0.6 μm at low excitation intensity to 0.75 μm for $\Phi \approx 80$ kW cm^{-2}. Examination of the different values for τ_D recovered using different fitting methods shows that they are similar only at very low light flux (Figure 4c). As soon as photobleaching kicks in ($\Phi >$ 10 kW cm^{-2}), each fitting method returns a different value for τ_D, the highest being obtained when using Equation (6). This means that in the presence of photobleaching, analysis methods not taking it into account cannot be trusted to yield a proper value for τ_D. As a rule, the residence time of the particles in the detection volume is limited by the shortest of the relevant characteristic times in the system, and analysis of the corresponding ACF will yield a precise value only for this shortest time. Thus, in the presence of severe photobleaching, τ_P is measured precisely, but τ_D is not, and in the presence of fast beam scanning, τ_S is measured precisely, but τ_D is not.

The increasing influence of photobleaching with excitation intensity is further evidenced by comparing the PCHs recorded with (gray symbols) and without (black symbols) beam scanning (Figure 4b). While at very low excitation intensity the two PCHs are virtually identical, at high excitation intensity there is a clear shift of the distribution towards higher photon counts in the presence of beam scanning. The PCHs obtained in the presence of beam scanning were analyzed by the FIDA method while letting the two parameters that describe the geometry of the detection volume, A_0 and A_1, vary. Both parameters were found to increase with increasing excitation intensity. When the PCHs recorded without beam scanning were analyzed in the same way, the values obtained for A_0 were found to be similar to those obtained with beam scanning, while the values obtained for A_1 were not, and the discrepancy increased with excitation power. We attribute this behavior to photobleaching: As the photobleaching becomes more severe, the fluorophore concentration across the detection volume becomes nonuniform, and this results in an incorrect evaluation of the geometrical parameters.

when fitting the ACFs [Eq. (6)], τ_D increases monotonously with the excitation power (Figure 4c) as expected from optical saturation. From this fit, the characteristic photobleaching time τ_P (shown in Figure 4c) and the associated amplitude A are obtained. While it is expected that $A \approx 0.8$, we found that it varied between $A \approx 0$ at low excitation intensity and $A \approx 0.5$ for $\Phi \approx 70$ kW cm^{-2}. This discrepancy probably indicates that in the range of excitation intensity we explored (where $\tau_P > \tau_D$), the photobleaching effect is too weak for the fit to be reliable. In contrast, other groups that successfully used Equation (6) to fit correlation data worked at much higher light energy fluxes (where $\tau_P < \tau_D$) and recovered $A \approx 0.8$.[14,15]

In the presence of circular beam scanning, photobleaching is reduced, and the dominant process affecting the ACFs (Figure 4a, gray curves) is optical saturation. This is evidenced by the monotonous increase of both the characteristic scanning time τ_S and the characteristic diffusion time τ_D (shown in Figure 3c), obtained by fitting these ACFs with a diffusion-velocity

Thus, because the correct values for A_0 and A_1 cannot be obtained when photobleaching is present, we subsequently analyzed PCHs without beam scanning while fixing the values of A_0 and A_1 to the values obtained with beam scanning at the same intensity. The results of these fits (number of molecules in the detection volume and specific brightness) are shown in Figure 4d. In the absence of photobleaching (i.e. at low excitation intensity or in the presence of beam scanning), the PCHs are perfectly described by super-Poissonian statistics for a single species of fluorophore, as expected. In addition, and in agreement with the simulations performed by Dix et al.,[16] in the presence of photobleaching (high excitation intensity, no scanning) the PCH is apparently still governed by super-Poissonian statistics, but the apparent number of molecules decreases by about 30%, while only a 5% decrease in the specific brightness of the dye is detected (Figure 4d).

To see how analysis of the fluctuation might change for slowly diffusing particles, ACF and PCH curves were recorded for a sample of LUVs containing a small amount of the lipophilic dye DiD. Representative curves, obtained for $\Phi = 10 \, \mathrm{kW \, cm^{-2}}$, are shown in Figure 5. For the vesicles, photo-
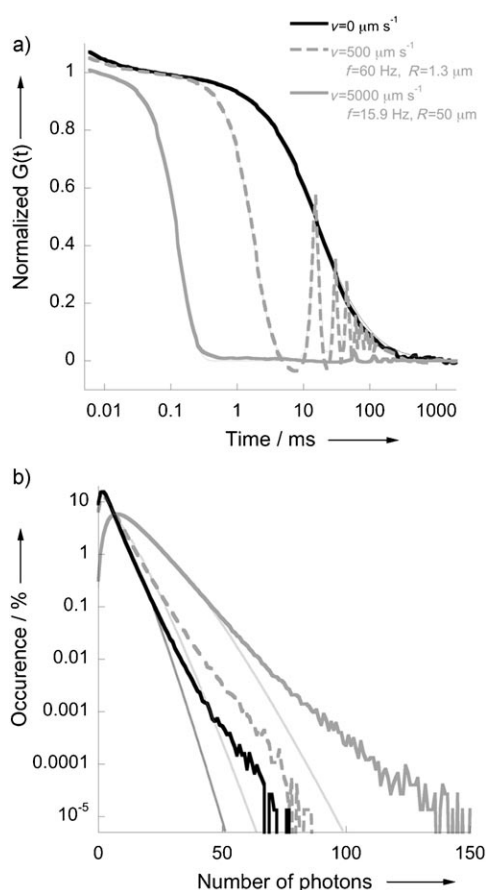
Figure 5. a) Autocorrelation functions obtained for DiD-labeled vesicles with and without beam scanning, for a light energy flux $\Phi = 10 \, \mathrm{kW \, cm^{-2}}$. b) Photon counting histograms corresponding to the autocorrelation curves shown in (a). Thick lines are representative 5 min measurements. Thin lines are fit as explained in the text.

bleaching is present even at this low excitation intensity, and

its effects can be detected in the PCHs (Figure 5b), which show that more photons are detected with beam scanning (gray curves) than without (black curve). The PCHs were fit with a single-component model. Although agreement with the experimental data is not perfect (which was expected, because the vesicles have a distribution of specific brightness) we were able to recover the dominant trends in terms of concentration and specific brightness. We observed that both the apparent concentration and the specific brightness of the particles increased significantly in the presence of beam scanning (by ≈100% and ≈70%, respectively, when increasing the beam velocity from 0 to 5000 $\mathrm{\mu m \, s^{-1}}$). The contrast to the case of the dye is worth pointing out: the vesicles each carry several fluorophores, thus photobleaching results in an actual reduction of their specific brightness, and this is reflected in the FIDA results.

The corresponding ACFs are shown in Figure 5a. In the absence of beam scanning, a simple diffusion model [Eq. (3)] fails to account for the data, at least in part because of photobleaching. However, because we also expect a certain distribution in the size of the vesicles, we cannot use Equation (6) to evaluate the relative effects of diffusion and photobleaching. The characteristic diffusion time $\tau_D = 15.4$ ms returned by the simple diffusion model should consequently be treated as the lower limit for the actual characteristic diffusion time. Indeed, the extruded vesicles used in our experiments have a 50 nm radius, and according to the Stokes–Einstein equation, they should have a diffusion coefficient $D \approx 4 \, \mathrm{\mu m^2 \, s^{-1}}$, corresponding to $\tau_D \approx 30$ ms for $w_0 \approx 0.7 \, \mathrm{\mu m}$. The ACFs obtained in the presence of circular beam scanning look different depending on the relative values of $2\pi f$ and $1/\tau_D$, as predicted by Equation (4). For $f \gg f_t = 1/(2\pi\tau_D) \approx 10$ Hz, oscillations are clearly visible in the ACF (Figure 5a, dashed gray curve) because the same fluorophores are observed in the detection volume after a 2π revolution of the beam.[25] In this case, the ACF is well fit by Equation (4), yielding $f = 65$ Hz and $R = 0.9 \, \mathrm{\mu m}$ (where the value of w_0 obtained from the experiments with the dye has been used to calculate R), which is in reasonable agreement with the actual scanning parameters ($f = 60$ Hz, $R = 1.3 \, \mathrm{\mu m}$). As f approaches 10 Hz, the amplitude of these oscillations becomes negligible (Figure 5a, solid gray curve), since fluorophores have time to diffuse away before the beam can complete a full revolution, and the ACF can be fit using the simplified Equation (5). In that case, we simply retrieve the characteristic residence time due to scanning, which was found to be similar to that obtained for the dye experiments.

In summary, the following remarks can be made from the inspection of the correlation data shown in Figure 4 and Figure 5. First, in the range of excitation power usually used in FCS experiments ($\Phi \approx 1$–20 $\mathrm{kW \, cm^{-2}}$), photobleaching effects are hardly noticeable for very quickly diffusing fluorophores such as dyes, while they are very severe for slowly diffusing particles such as vesicles. Second, photobleaching is difficult to diagnose from the analysis of a single ACF, but it is evidenced by a shift of the PCH towards higher photon counts upon activation of beam scanning.

Optimization of the Scanning Parameters for Long-Term Photobleaching Suppression

In order to experimentally assess the influence of scanning parameters on the reduction of long-term photobleaching effects, we measured the average fluorescence intensity collected from a LUV sample while scanning the beam over circular trajectories with different radii but with a fixed scanning speed. The constant scanning speed ensured that the residence time of the fluorophores remained the same. This way, short-term photobleaching effects remained the same, and long-term photobleaching effects could be investigated. The result of this experiment is shown in Figure 6. For the studied
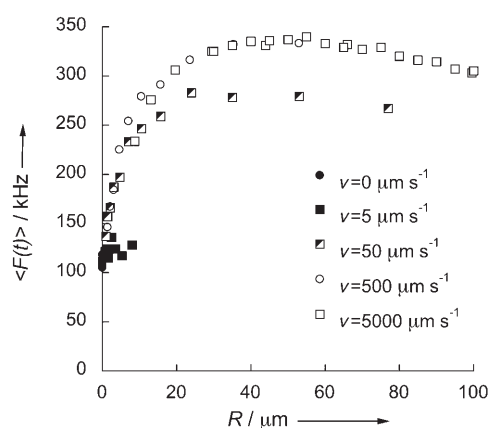
Figure 6. Fluorescence intensity measured from a vesicle sample with circular beam scanning at constant speed, as a function of the beam scanning radius ($\Phi = 10 \text{ kW cm}^{-2}$).

system, the critical velocity $v_c = 2D/w_0$, above which we expect a reduction of the long-term photobleaching effects, can be estimated to be $v_c \approx 10 \text{ μm s}^{-1}$ (since $w_0 \approx 0.7 \text{ μm}$ and $D \approx 4 \text{ μm}^2\text{s}^{-1}$). Indeed, for $v < 10 \text{ μm s}^{-1}$ (filled symbols), we observe that the fluorescence intensity collected at all radii remains very similar to the fluorescence intensity collected in the absence of beam scanning. On the other hand, for $v > 10 \text{ μm s}^{-1}$ (half-filled and empty symbols), the fluorescence intensity rapidly increases with scanning radius. This confirms that for $v < v_c$, the velocity of the beam is not sufficient to avoid the influence of fluorophores that have just been photobleached and are still in the proximity of the detection volume. For $v > v_c$, all curves show the following trend: As the scanning radius is increased from $R \approx 0$ to $R \approx 30 \text{ μm}$, the recorded fluorescence increases steeply. It then reaches a plateau between $R \approx 30 \text{ μm}$ and $R \approx 60 \text{ μm}$ and finally starts slowly decreasing above $R \approx 60 \text{ μm}$. The reduced intensity observed below $R \approx 30 \text{ μm}$ can be attributed to the presence of a photobleaching hole. Indeed, the curves shown in Figure 6 have a very similar behavior to those in Figure 3 f, which showed the apparent number (because of the creation of a photobleaching hole) of particles as a function of scanning radius. Each point in Figure 6 corresponds to the average of three different 10-s measurements, meaning that the total measurement duration

was about 30 s. Considering $D \approx 4 \text{ μm}^2\text{s}^{-1}$ for the vesicles, we expect the photobleaching hole to have a radius $R_h = \sqrt{4Dt} \approx 20 \text{ μm}$, which is very close to what we actually observe. The influence of the photobleaching hole can thus be avoided by choosing $R > R_h$, or it can be reduced by limiting the duration of the measurements, by allowing the sample to rest between measurements, or by taking consecutive measurements in different places in the sample. On the other hand, the slow decrease in fluorescence count rate observed for radii $R > R_i \approx 60 \text{ μm}$ at all scanning speeds can be attributed to comatic aberrations. This type of optical aberration occurs when the laser beam is off axis and results in a distortion of the point spread function, which becomes larger as the angle between the laser beam and the optical axis increases. This effect is negligible at small scanning radii, but causes a visible reduction in the fluorescence count rate and brightness per molecule for $R > R_i$. The value of R_i obviously depends on the optical components used for collecting the fluorescence, in particular of the objective lens. We finally note that the plateau reached for $v = 50 \text{ μm s}^{-1}$ is lower than for the two higher scanning speeds. This we attribute to the fact that short-term photobleaching effects must still be present at this speed; in other words, $v = 50 \text{ μm s}^{-1} < v_P$, as discussed in the next section.

In summary, this experimental data confirms that photobleaching can be reduced for $v > v_c$, and emphasizes the importance of using a scanning radius larger than the radius of the photobleaching hole, which can also be reduced by decreasing the measurement duration.

Influence of the Scanning Velocity on Short-Term Fluorophore Photobleaching

To verify that an increase in the scanning speed results in an increase in measured fluorescence according to Equation (10), we measured the average fluorescence intensity as a function of scanning speed for both a dye sample and a vesicle sample (Figure 7a). Agreement with Equation (10) is expected only if the scanning conditions have been chosen such that long-term photobleaching effects are negligible. Consequently, for these measurements the scanning parameters were selected according to the discussion in the previous sections. Specifically, we kept $v > v_c \approx 10 \text{ μm s}^{-1}$, $R > R_h \approx 20 \text{ μm}$, $R < R_i \approx 60 \text{ μm}$ and $f < f_t \approx 30 \text{ Hz}$ for the vesicle sample. For the dye sample, although we estimated that $v_c \approx 1000 \text{ μm s}^{-1}$, long-term photobleaching effects are negligible in all scanning conditions because the large diffusion coefficient of the dye ensures that any photobleaching hole will be very shallow. Thus, in that case the only scanning requirement is $R < R_i \approx 60 \text{ μm}$.

The average fluorescence intensity measured for Alexa 633 at low excitation power ($\Phi = 8 \text{ kW cm}^{-2}$) remained constant over the large range of scanning speeds explored, a sign of the absence of photobleaching effects. On the other hand, at a comparable excitation power ($\Phi = 10 \text{ kW cm}^{-2}$), the influence of photobleaching is clearly visible in the fluorescence intensity curve recorded for the vesicles. Using a very high excitation power ($\Phi = 70 \text{ kW cm}^{-2}$) resulted in visible photobleaching effects for both the vesicles and the dye, in agreement with the
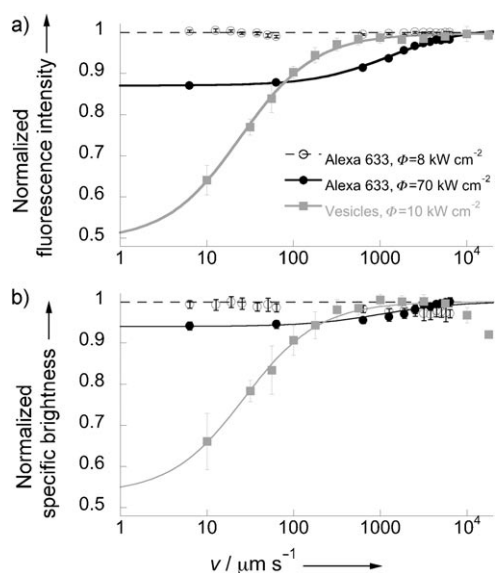
Figure 7. a) Normalized fluorescence intensity as a function of scanning velocity for different samples. The thick continuous lines represent fits of the data with Equation (10). The thin dashed line is a guide for the eyes. b) Normalized specific brightness obtained by FIDA analysis for the same samples. Lines are guides for the eyes. ○ Alexa 633 $\Phi=8$ kW cm^{-2}, ● Alexa 633 $\Phi=70$ kW cm^{-2}, ■ vesicles $\Phi=10$ kW cm^{-2}.

fluorescence fluctuation data shown above (Figure 4). As expected from Equation (10), the two curves showing evidence of photobleaching both reach a plateau above a certain velocity, which was different in each case. This confirms the existence of a crossover velocity v_P, above which short-term photobleaching effects become negligible.

It is possible to obtain more quantitative information about the photobleaching taking place in the sample by fitting the experimental data with Equation (10). For the vesicle data shown in Figure 7a, we found $\tau_D=38\pm6$ ms, whereas the characteristic photobleaching time of the DiD fluorophore was found to be $\tau_P=31\pm2$ ms. Therefore, under these experimental conditions $\tau_P\approx\tau_D$, so that in the absence of beam scanning about half of the DiD fluorophores photobleach during their transit through the detection volume. As a result, there was a $\approx50\%$ decrease in total fluorescence intensity recorded for this sample at low scanning speeds. This is in contrast to what was observed for the dye. At the highest excitation intensity explored, $\Phi=70$ kW cm^{-2}, the characteristic diffusion time estimated for the dye was $\tau_D=460\pm50$ μs, while the estimated characteristic photobleaching time was $\tau_P=2.0\pm0.2$ ms. The fact that $\tau_D<\tau_P$ means that even at this very high excitation power, the majority of the fluorophores remained fluorescent throughout their passage through the detection volume. This is consistent with the relatively modest intensity decrease observed at low scanning speeds.

The characteristic photobleaching time $\tau_P=2$ ms estimated in this manner for the Alexa dye for $\Phi=70$ kW cm^{-2} is significantly different from the value $\tau_P=0.5$ ms obtained from analysis of the ACF using Equation (6) (Figure 4). Since photobleaching is not predominant in these conditions ($\tau_P>\tau_D$), the estimate of this parameter from the ACF might be inaccurate. This

argument is supported by the fact that the amplitude A recovered from the same analysis was less than the expected value (0.8). Furthermore, we assumed $S\approx1$ to derive Equation (10), so that the values of τ_P obtained using this equation might present a systematic deviation from the actual value. However, since the dependence of the residence time on S is weak, this deviation should be small. In contrast to what is observed for τ_P, the characteristic diffusion time obtained for the dye is reasonably close to that obtained by ACF analysis ($\tau_D=460$ μs as compared to $\tau_D=564$ μs), and the value $\tau_D=38$ ms obtained for the vesicles is much closer to the characteristic diffusion time expected in these conditions for a spherical particle of radius 50 nm, $\tau_D=28$ ms, than was the value $\tau_D=15.4$ ms obtained from the analysis of the corresponding ACF.

The specific brightness of both the dye and the vesicles, as estimated using one-component FIDA, is shown in Figure 7b. For the dye, the specific brightness is lower at low beam velocity in the presence of photobleaching. However, this decrease is not as important as the decrease in total intensity. In contrast, in the case of the vesicles, the decrease in specific brightness at low scanning speed exactly matches the decrease in total fluorescence intensity. This is because vesicles carry several DiD fluorophores, about half of which photobleach during transit through the detection volume, resulting in an apparent specific brightness of the vesicle that is lower than that in the absence of photobleaching.

In conclusion, our experimental data confirms that circular beam scanning allows the elimination of short-term photobleaching effects. We find that, as expected from our simple model [Eq. (10)], the measured average fluorescence intensity increases to its maximum value for $v>v_P$. Fitting this data allows us to estimate the characteristic diffusion time τ_D and the photobleaching time τ_P.

Influence of the Excitation Power on Fluorophore Photobleaching.

We next looked into the excitation-power dependence of the photobleaching process. Figure 8 shows the average fluores-
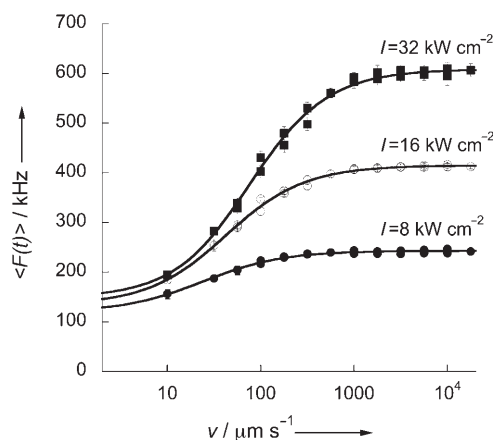

Figure 8. Fluorescence intensity collected from a vesicle sample plotted as a function of beam velocity for different excitation powers. Lines represent fits of the data with Equation (10).

cence intensity recorded for the vesicles as a function of scanning speed for several different excitation powers. As the excitation power is increased, the effective photobleaching rate increases, and photobleaching effects become more noticeable. This is evidenced in the relative increase in average fluorescence intensity as the scanning speed is increased from $10\ \mu m\,s^{-1}$ to $30\ mm\,s^{-1}$, which gets larger when the excitation power is increased. Additionally, the value of the scanning speed at which we observe a crossover between important and negligible photobleaching effects, v_P, increases as expected with the excitation power. This underscores the importance of choosing scanning parameters according to specific experimental conditions in order to efficiently reduce the effects of photobleaching.
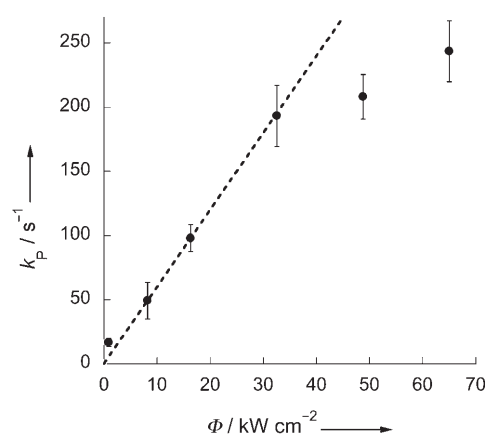
The reduction of the photobleaching effects obtained in the presence of optimal beam scanning, defined by the scanning conditions at which the measured fluorescence intensity is at a maximum, is illustrated in Figure 9, where the specific brightness of the vesicles with and without beam scanning is compared.
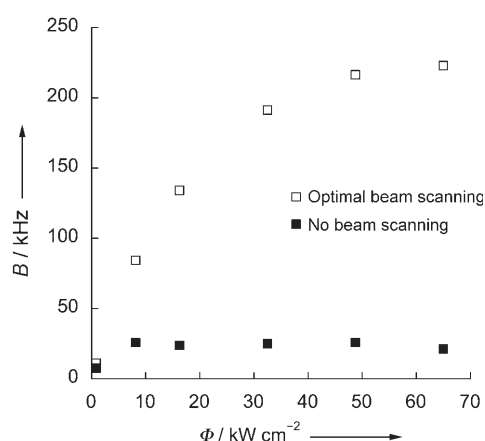
Figure 9. Specific brightness of the DiD-labeled vesicles, obtained using FIDA to analyze the PCHs recorded for an immobile beam (filled symbols) and with optimal beam scanning (empty symbols), as a function of excitation intensity.

pared. In the absence of beam scanning, the specific brightness of the vesicles reaches its maximum value at $\Phi = 10\ kW\,cm^{-2}$ due to short-term photobleaching. But in the presence of optimal beam scanning, photobleaching is reduced such that specific brightness continues to increase until $\Phi = 50\ kW\,cm^{-2}$. This data very strikingly demonstrates the usefulness of beam scanning to recover the proper specific brightness of slow particles.

The effective photobleaching rate of the DiD fluorophore, k_P, obtained from the analysis of different intensity curves using Equation (10), is shown in Figure 10 as a function of the light-energy flux. At low flux, k_P increases linearly with Φ, but above $\Phi \approx 40\ kW\,cm^{-2}$ a slight saturation is observed. We expect the photobleaching rate to deviate from a linear behavior at higher flux, either because of population saturation of the first singlet excited state (in which case the photobleaching rate should plateau) or because of population of higher-energy ex-

Figure 10. Effective rate associated with photobleaching of the DiD fluorophore as a function of light energy flux. The dashed line represents a linear fit of the data for $\Phi < 40\ kW\,cm^{-2}$.

cited states (in which case the photobleaching rate should start increasing faster).[15] The first effect seems to predominate in the case of the DiD fluorophore in the range of energy flux used in this study. We nevertheless expect the second effect to become predominant at higher flux.[15] By fitting the data to Equation (7) in the linear regime ($\Phi < 40\ kW\,cm^{-2}$), we obtained an estimate for the photobleaching cross section of DiD at 637 nm, $\sigma_P = 1.3 \pm 0.2 \times 10^{-13}\ \mu m^2$. This value is comparable to the value obtained for the photobleaching cross-section of EGFP, $\sigma_P = 0.7 \times 10^{-13}\ \mu m^2$, and about one order of magnitude smaller than that obtained for fluorescein, $\sigma_P = 24 \times 10^{-13}\ \mu m^2$.[36] The photobleaching quantum yield, $Q_P = \sigma_P/\sigma_A$, can be calculated by considering the absorption cross-section of the dye, $\sigma_A = 2.6 \times 10^{-8}\ \mu m^2$ at 637 nm. We obtain $Q_P = 6.1 \times 10^{-5}$, a value falling in the range reported for Coumarin dyes ($Q_P \approx 10^{-4}$–10^{-3}) and Rhodamine dyes ($Q_P \approx 10^{-7}$–10^{-6}).[15] The DiD fluorophore thus appears to be a rather photostable fluorophore. This implies that the large photobleaching effect observed for the vesicles is due to their slow diffusion rather than to an abnormally high susceptibility of DiD to photobleaching.

Conclusions

Our calculations suggest that linear beam scanning is a very efficient way to reduce both long-term and short-term photobleaching effects in fluorescence fluctuation experiments. While scanning the beam linearly for more than $\approx 100\ \mu m$ is not practical, circular beam scanning makes it possible to maintain a constant scanning speed over a potentially infinite trajectory and offers the advantage of tractable ACF analysis. We have shown that three different effects, summarized in Figure 11, must be considered when trying to optimize circular scanning conditions in order to reduce photobleaching. First, to reduce long-term photobleaching effects one must make sure that $v > v_c$ (to overcome the diffusion of newly photobleached particles) and that $R > R_h$ and $f < f_t$ to avoid the formation of a photobleaching hole around the detection volume. Second, to reduce short-term photobleaching effects, one must have $v > v_P$ to decrease the residence time of the
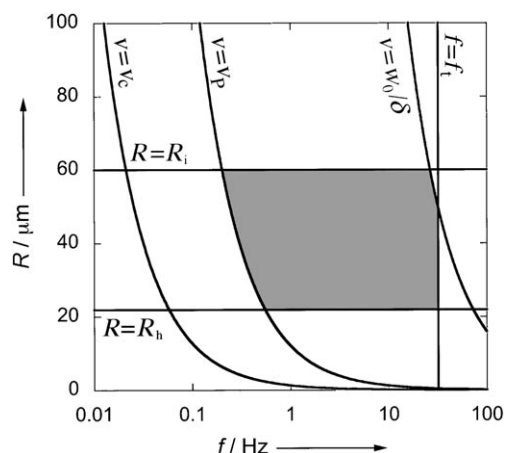
Figure 11. Summary of the circular scanning conditions necessary in order to circumvent photobleaching. Short-term photobleaching is negligible for $v > v_p$, while long-term photobleaching is negligible for $v > v_c$, $R > R_h$ and $f < f_t$. Optical aberrations start significantly reducing the specific brightness of fluorophores for $R > R_i$, and PCH analysis becomes inaccurate for $v > w_0/\delta$. The gray shaded area indicates the useful parameter region for performing fluorescence fluctuation measurements free of photobleaching effects. The values of v_c, R_h, f_t, v_p and w_0/δ have been calculated using: $D = 2 \ \mu m^2 s^{-1}$, $k_P = 200 \ s^{-1}$, $w_0 = 0.5 \ \mu m$, $t = 60 \ s$, $\delta = 50 \ \mu s$.

particles in the excitation volume below the characteristic photobleaching time τ_P. Third, technical limitations specific to each instrument must be determined. In particular, one must have $R < R_i$ where R_i is determined by the properties of the objective lens. Finally, the residence time must be maintained above the sampling time δ used to construct the PCH, that is, $v < w_0/\delta$.

Although the presence of a photobleaching hole has been described in the context of the slow diffusion of proteins in a 2D lipid membrane[19] and in the context of FCS measurements carried out in samples with limited volumes,[17,18,34] our study is the first to point out the influence of the photobleaching hole in the case of beam scanning. Our study was restricted to single-photon excitation. For multiphoton excitation, we expect the conditions necessary to avoid long-term photobleaching effects to relax, as the decisive influence of out-of-focus photobleaching is absent in that case. However, the conditions necessary to avoid short-term photobleaching effects should become even more stringent, as multiphoton excitation has been shown to result in higher effective photobleaching cross sections.[37]

The influence of fluorophore photobleaching on the outcome of FCS experiments has been well-studied,[15,17–20,38] but only very few studies have addressed the same question for the outcome of PCH analysis.[16,21] Since beam scanning allows precise regulation of the fraction of photobleached fluorophores present in the detection volume, this method presents a rare opportunity to study the influence of short-term photobleaching on the PCH and on the result of FIDA analysis, something beyond the scope of the present study. We do note, however, that in agreement with numerical simulations,[16] photobleaching causes a reduction in both the apparent particle concentration and particle specific brightness obtained by FIDA.

The important message of this study is that in the case of slowly diffusing objects, photobleaching drastically affects the result of fluorescence fluctuation experiments, even when using photostable dyes and modest excitation powers. The most striking effect is a dramatic reduction of the apparent specific brightness of multifluorophore particles as obtained by FIDA from the PCH in the presence of photobleaching, with obvious consequences for all studies relying on analysis of the PCH for determination of the specific brightness of slow fluorescent particles. Since our study shows that to be efficient against long-term photobleaching, the scanning radius must be sufficiently large, circular beam scanning will not help reduce photobleaching in cells, and imaging methods such as image correlation spectroscopy and raster image correlation spectroscopy will be the techniques of choice to study slow cellular diffusion. On the other hand, circular beam scanning is a very efficient method to reduce photobleaching in open systems. In particular, it will be most helpful for avoiding photobleaching when measuring the specific brightness and diffusion of large particles in solution.

[1] A. D. Mehta, M. Rief, J. A. Spudich, D. A. Smith, R. M. Simmons, *Science* **1999**, *283*, 1689–1695; Y. Sako, T. Yanagida, *Nat. Rev. Mol. Cell Biol.* **2003**, S1–S5; S. Weiss, *Nat. Struct. Biol.* **2000**, *7*, 724–729.

[2] P. Cluzel, M. Surette, S. Leibler, *Science* **2000**, *287*, 1652–1655; H. Murakoshi, R. Iino, T. Kobayashi, T. Fujiwara, C. Ohshima, A. Yoshimura, A. Kusumi, *Proc. Natl. Acad. Sci. USA* **2004**, *101*, 7317–7322; A. Yildiz, J. N. Forkey, S. A. McKinney, T. Ha, Y. E. Goldman, P. R. Selvin, *Science* **2003**, *300*, 2061–2065; X. Zhuang, L. E. Bartley, H. P. Babcock, R. Russell, T. Ha, D. Herschlag, S. Chu, *Science* **2000**, *288*, 2048–2051.

[3] R. Rigler, U. Mets, J. Widengren, P. Kask, *Eur. Biophys. J.* **1993**, *22*, 169–175.

[4] M. Wachsmuth, W. Waldeck, J. Langowski, *J. Mol. Biol.* **2000**, *298*, 677–689.

[5] R. H. Kohler, P. Schwille, W. W. Webb, M. R. Hanson, *J. Cell Sci.* **2000**, *113*, 3921–3930.

[6] P. Kask, P. Piksarv, M. Pooga, U. Mets, E. Lippmaa, *Biophys. J.* **1989**, *55*, 213–220.

[7] G. Bonnet, O. Krichevsky, A. Libchaber, *Proc. Natl. Acad. Sci. USA* **1998**, *95*, 8602–8606.

[8] S. A. Kim, K. G. Heinze, M. N. Waxham, P. Schwille, *Proc. Natl. Acad. Sci. USA* **2004**, *101*, 105–110.

[9] W. W. Webb, *Appl. Opt.* **2001**, *40*, 3969–3983; E. Haustein, P. Schwille, *Methods* **2003**, *29*, 153–166.

[10] N. O. Petersen, P. L. Hoddelius, P. W. Wiseman, O. Seger, K. E. Magnusson, *Biophys. J.* **1993**, *65*, 1135–1146; M. A. Digman, P. Sengupta, P. W. Wiseman, C. M. Brown, A. R. Horwitz, E. Gratton, *Biophys. J.* **2005**, *88*, L33–36.

[11] H. Qian, E. L. Elson, *Biophys. J.* **1990**, *57*, 375–380.

[12] Y. Chen, J. D. Muller, P. T. So, E. Gratton, *Biophys. J.* **1999**, *77*, 553–567.

[13] P. Kask, K. Palo, D. Ullmann, K. Gall, *Proc. Natl. Acad. Sci. USA* **1999**, *96*, 13756–13761.

[14] J. Widengren, R. Rigler, *Bioimaging* **1996**, *4*, 149–157.

[15] C. Eggeling, J. Widengren, R. Rigler, C. A. Seidel, *Anal. Chem.* **1998**, *70*, 2651–2659.

[16] J. A. Dix, E. F. Hom, A. S. Verkman, *J. Phys. Chem. B* **2006**, *110*, 1896–1906.

[17] M. Wachsmuth, T. Weidemann, G. Muller, U. W. Hoffmann-Rohrer, T. A. Knoch, W. Waldeck, J. Langowski, *Biophys. J.* **2003**, *84*, 3353–3363.

[18] A. Delon, Y. Usson, J. Derouard, T. Biben, C. Souchier, *Biophys. J.* **2006**, *90*, 2548–2562.

[19] J. Widengren, P. Thyberg, *Cytometry Part A* **2005**, *68*, 101–112.

[20] A. Delon, Y. Usson, J. Derouard, T. Biben, C. Souchier, *J. Fluoresc.* **2004**, *14*, 255–267.

[21] M. Caccia, E. Camozzi, M. Collini, M. Zaccolo, G. Chirico, *Appl. Spectrosc.* **2005**, *59*, 227–236.

[22] A. G. Palmer, III, N. L. Thompson, *Biophys. J.* **1987**, *51*, 339–343.

[23] N. O. Petersen, *Biophys. J.* **1986**, *49*, 809–815.

[24] M. Eigen, R. Rigler, *Proc. Natl. Acad. Sci. USA* **1994**, *91*, 5740–5747.

[25] K. M. Berland, P. T. So, Y. Chen, W. W. Mantulin, E. Gratton, *Biophys. J.* **1996**, *71*, 410–420.

[26] U. Haupts, M. Rudiger, S. Ashman, S. Turconi, R. Bingham, C. Wharton, J. Hutchinson, C. Carey, K. J. Moore, A. J. Pope, *J. Biomol. Screening* **2003**, *8*, 19–33.

[27] C. Eggeling, P. Kask, D. Winkler, S. Jager, *Biophys. J.* **2005**, *89*, 605–618.

[28] Q. Ruan, M. A. Cheng, M. Levi, E. Gratton, W. W. Mantulin, *Biophys. J.* **2004**, *87*, 1260–1267; J. Ries, P. Schwille, *Biophys. J.* **2006**, *91*, 1915–1924.

[29] P. Kask, K. Palo, N. Fay, L. Brand, U. Mets, D. Ullmann, J. Jungmann, J. Pschorr, K. Gall, *Biophys. J.* **2000**, *78*, 1703–1713.

[30] T. Winkler, U. Kettling, A. Koltermann, M. Eigen, *Proc. Natl. Acad. Sci. USA* **1999**, *96*, 1375–1378.

[31] D. Magde, E. Elson, W. W. Webb, *Phys. Rev. Lett.* **1972**, *29*, 705–708.

[32] D. Magde, W. W. Webb, E. L. Elson, *Biopolymers* **1978**, *17*, 361–376; M. Gosch, H. Blom, J. Holm, T. Heino, R. Rigler, *Anal. Chem.* **2000**, *72*, 3260–3265.

[33] P. S. Dittrich, P. Schwille, *Appl. Phys. B* **2001**, *73*, 829–837.

[34] J. Mertz, *Eur. Phys. J. D* **1998**, *3*, 53–66.

[35] I. Gregor, D. Patra, J. Enderlein, *ChemPhysChem* **2005**, *6*, 164–170.

[36] Y. Chen, J. D. Muller, K. M. Berland, E. Gratton, *Methods* **1999**, *19*, 234–252.

[37] G. H. Patterson, D. W. Piston, *Biophys. J.* **2000**, *78*, 2159–2162.

[38] C. Eggeling, A. Volkmer, C. A. Seidel, *ChemPhysChem* **2005**, *6*, 791–804.